Using surface force apparatus, diffusion and velocimetry to measure slip lengths

Cédric Bouzigues, Lyderic Bocquet, Elisabeth Charlaix, Cécile Cottin-Bizonne, Benjamin Cross, Laurent Joly, Audrey Steinberger, Christophe Ybert, Patrick Tabeling

Using surface force apparatus, diffusion and velocimetry to measure slip lengths

C. I. Bouzigues[1], L . B ocquet[2], E . C harlaix[2], C. Cottin-Bizonne[2], B. Cross[2], L. Joly[2], A. Steinberger[2], C. Ybert[2] and P. Tabeling[1,*]

[1]*Microfluidics, MEMs and Nanostructures Laboratory, CNRS UMR 7083 ESPCI, 10 rue Vauquelin, 75005 Paris, France*
[2]*Laboratoire PMCN, Université Lyon 1, CNRS UMR 5586, 69622 Villeurbanne Cedex, France*

Determining the slip lengths for liquids flowing close to smooth walls is challenging. The reason lies in the fact that the scales that must be addressed range between a few and hundreds of nanometres. Several techniques have been used over the last few years. Here, we consider three of them based on surface force apparatus, diffusion and velocimetry, respectively. The descriptions offered here incorporate recent instrumental progress made in the field.

Keywords: slip length; force apparatus; hindered diffusion; velocimetry

1. Introduction

Much has been done over the last few years to understand the slip phenomena occurring at liquid–solid interfaces. To make a long story short, the general view at the moment is that close to non-wetting walls a depletion layer is formed, which lubricates the liquid and in turn favours slippage. The magnitude of this effect is measured through the slip length, a quantity that was defined first by Navier in the middle of the nineteenth century. The relationship that defines the slip lengths is the following hydrodynamic boundary condition (h.b.c.):

$$u_{|_{z=0}} = b \frac{\partial u}{\partial z}_{|_{z=0}}, \tag{1.1}$$

where u is the velocity parallel to the wall; z is the coordinate normal to the wall; and b is the so-called slip length. Sometimes, this quantity is also called the 'Navier length' (Navier 1822; Tabeling 2003). The existence of a non-zero slip length is interesting and troublesome for the following reasons.

— Interesting because for practical reasons it would certainly be valuable to devise and build systems with large slip lengths. If this were possible, liquids would flow through channels for free, since, at a fixed flow rate, fluid

* Author for correspondence (patrick.tabeling@espci.fr).

dissipation decreases as the inverse of the slip length (Tabeling 2003). This remark is worth being made with the advent of micro-exchangers and the development of nanofluidics where, in both cases, driving liquids through micro- or nanochannels requires large pressure differences, which in turn raises difficult practical issues.

— Troublesome because it has been repeatedly said that liquids cannot slip over solid surfaces (Navier 1822). Should it be so, the mechanical balance between the forces induced by the tangential stress and the pressure forces would imply the liquid remains at rest. The existence of a slippage thus questions a belief that the fluid mechanical community has conveyed throughout the last century.

Historically, the first serious hints concerning the existence of the slippage phenomena came over the last decade with the development of numerical computation (Thompson & Troian 1997; Barrat & Bocquet 1999). Essentially, these simulations showed that, when the liquid–wall attraction is less than the liquid self-attraction, a depletion layer develops close to the wall. In this layer, viscosity is reduced and the flow is lubricated. Thus, as mentioned above, one obtains a slippage effect. The orders of magnitudes of the slip lengths obtained numerically were typically a few nanometres. This estimate lies well above the intermolecular scale, but in the meantime raises challenges for its experimental determination.

There are essentially four techniques of the measurement of the slip length.

(i) *Surface force machine*. This measures the force–velocity relationship as the two surfaces approach each other, down to a few nanometres. Using hydrodynamic theory, one may infer the slip length from the force–velocity plot.

(ii) *Pressure drop analysis*. This consists in determining the pressure–flow rate relationship for a flow driven through a microchannel. Using the hydrodynamic theory, one may infer the slip length from the pressure–flow rate plot.

(iii) *Brownian motion analysis*. This consists in analysing the Brownian motion of nanoparticles extremely close to a wall. From the measurement of the diffusion constant, one may infer the slip length.

(iv) *Velocimetry close to the wall*. This consists in measuring the velocity profile close to the wall. By extrapolating these profiles down to the wall, one infers the slip length.

Here, we report the sets of data obtained using three of these methods, labelled as (i), (iii) and (iv), respectively. It will appear that they provide consistent determination of the slip lengths, albeit substantially above numerical estimates. The pressure drop method is not extensively discussed in this paper and has been successfully used (Choi *et al.* 2003) to estimate the slip length at elevated shear rates (more than $10\,000\,\mathrm{s}^{-1}$). It is consequently difficult to quantitatively compare these results with other methods, which focus on the zero shear rate limit. However, extrapolation to this limit of results from pressure drop experiments reveals slip length values comparable (Choi *et al.* 2003) to those obtained from the studies detailed in this paper.

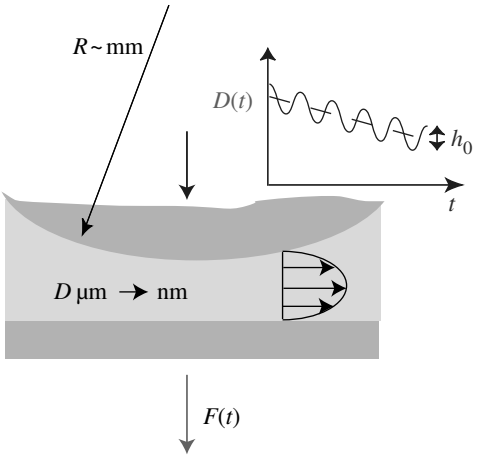

Figure 1. Schematic of a liquid confined between a sphere of radius R and a plane. In a dynamic surface force apparatus experiment, a sphere is moved towards a plane by superimposing a slow continuous drift and a harmonic motion of amplitude h_0. We measure separately the distance D between the surfaces and the static and oscillating force F acting on the plane. The velocity profile represented here at an instant t corresponds to a no-slip boundary condition on the sphere and the plane.

2. Surface force measurements

Figure 1 provides a sketch of the surface force measurement. The method is based on the measurement of the viscous force induced by a sphere moving orthogonally to a plane. From this measurement, it is possible to measure the slip length.

The surfaces studied here are either plain Pyrex or Pyrex that has been silanized by immersion in a mixture of 100 µl octadecyltrichlorosilane (OTS) and 60 ml toluene for approximately 2 hours. The peak-to-peak roughness of the surfaces is measured by atomic force microscopy (AFM) and is, for all surfaces, 1 nm over 10×10 µm^2 area. The liquid used is ultrapure water (Millipore, MilliQ, 18.2 MΩ cm). Water wets the plain Pyrex surfaces. The contact angle of water on the silanized surfaces measured by the sessile drop method is 105°. The contact angle hysteresis is less than 2°. Identical surfaces prepared with similar protocols have been used in all experiments presented in this paper and are referred to as hydrophilic and hydrophobic cases or surfaces, respectively.

The dissipation method is based on the direct measurement of the viscous force induced by a sphere moving orthogonally to a plane (figure 1). From this measurement, it is possible to measure the h.b.c. of a liquid at a solid wall.

We have specifically designed a dynamic surface force apparatus to investigate the hydrodynamics of confined liquids (Restagno *et al.* 2002). Water is confined between a sphere (of radius R of a few millimetres) and a plane. We measure the oscillating force $F(\omega)$ acting on the plane in response to a small oscillation (amplitude h_0) of the sphere in the direction normal to the plane at a frequency $\omega/2\pi$. We measure separately the distance D between the sphere and the plane. All experiments are performed in a clean and thermally isolated room.

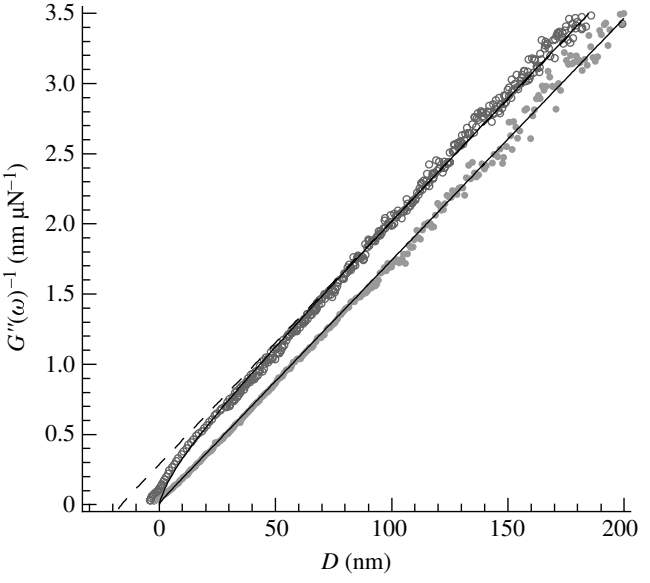

Figure 2. Inverse of the damping G''^{-1} as a function of the gap D, obtained for water confined between the plain Pyrex hydrophilic surfaces (filled circles) and between the asymmetric system plain Pyrex/OTS-coated Pyrex (open circles). The solid lines correspond to the theoretical expressions for a no-slip boundary condition or a slip length $b=19$ nm. The dashed line corresponds to the linear extrapolation of the signal in the case of slip; it intersects at the D-axis at a distance $b=19$ nm from the origin.

These two independent measurements allow an accurate determination of the complex force response $G(\omega)=F(\omega)/h_0$ at a mean distance D from the plane. The origin of the distances is the position where the plane and the sphere just come into contact. This position is obtained from the quasistatic interaction force between the surfaces with an error bar of approximately 2 nm. The imaginary part of the complex force response $G''(\omega)$ is the viscous damping due to the flow. It can be linked to the theoretical expression in the lubrication approximation (Vinogradova 1995) and can be used to determine the h.b.c. at the solid wall

$$\mathrm{Im}[G(\omega)] = G''(\omega) = 6\pi\eta\omega R^2 f^*/D,$$

where $f^*=1$ for a no-slip boundary condition and $f^* = (1/4)(1 + (6D/4b)\times [(1 + (D/4b))\ln(1 + (4b/D)) - 1])$ for a slippery surface with b the slip length on this surface.

We have measured the viscous damping for water confined between the plain Pyrex hydrophilic surfaces and between the asymmetric system plain Pyrex sphere/silanized hydrophobic plane. Details of these experiments can be found in Cottin-Bizonne *et al.* (2005). Figure 2 shows the experimental results for each system.

In the hydrophilic case, the inverse of the damping G''^{-1} as a function of the sphere–plane gap D is a straight line going through the origin, which corresponds to the well-known Reynolds force with a no-slip boundary condition ($f^*=1$) within a resolution of 3 nm. From the slope of the plot, we derive the viscosity of the confined water, $\eta=0.83\pm0.06$ mPa s, in good agreement with the viscosity of

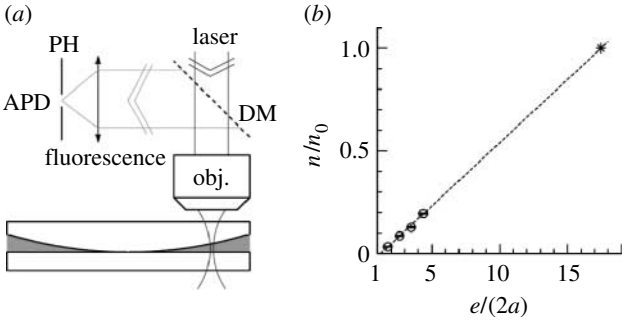

Figure 3. (*a*) Schematic of the experimental cell with FCS detection. Fluorescent colloids suspended in water are confined between a plane and a spherical lens. DM, dichroic mirror; obj., microscope objective; PH, pinhole; APD, avalanche photodiode. (*b*) Evolution of the bead number with the confinement. Symbol, polystyrene beads ($2a=210$ nm); dashed line, linear regression. Graph is taken from Joly *et al.* (2006).

water at 27°C. In the non-wetting case, the variation of G''^{-1} with D shows that slips develop at the wall. If we compare the experimental results with the theoretical expression (solid line in figure 2), we find a good agreement for a slip length $b=19\pm2$ nm. The linear extrapolation of the signal for large values of D (dashed line) intersects at the D-axis at a distance corresponding to the slip length b. It is also important to note that with this experiment it is easy to probe the linearity of the h.b.c.: a single value of the slip length accounts for the damping observed at all gap values extending from some nanometres to several hundreds of nanometres; we have also checked that the slip length does not depend on the frequency or the amplitude of the sphere motion. We could probe shear rates from 100 to 5×10^3 s^{-1} and find a linear h.b.c.

3. Thermal motion of confined colloids

In this section, we demonstrate an original experimental route whereby the nanohydrodynamics of liquids close to surfaces is explored *in the absence of any external forcing*. Rather than measuring the interfacial dissipation or the forced surface flow, we take advantage of the information already included in response to *thermal fluctuations* (Einstein 1905) to extract the interfacial dynamics. This technique, which is analogous—for surfaces—to the passive microrheology technique for bulk characterization (Mason & Weitz 1995), proves to be extremely sensitive as it allows us to reach an unprecedented resolution for an optical technique, namely a few nanometres on the slip length measurement.

We first describe the general principle of this approach. The diffusion dynamics of colloidal tracers is measured in a confined geometry between two solid surfaces of interest, using a home-built fluorescence correlation spectroscopy (FCS) device (figure 3*a*). Tracer dynamics is affected by confinement, and this dependence reflects the h.b.c. that apply on both solid substrates (Lauga & Squires 2005; Saugey *et al.* 2005). The results for different wetting properties of the solid substrates lead to measurable differences in the diffusion coefficient, allowing us to deduce the corresponding surface slippage.

Details of the set-up are reported by Joly *et al.* (2006). Below, we discuss only the most pertinent features of the experimental procedure.

While in bulk measurements, a confocal pinhole is inserted in the detection pathway to get a spatially defined measurement volume v, here the axial limits are set in practice by the two confining walls (figure 3*a*) so that $v=(\pi w^2)e$, where w is the beam waist radius and e is the wall-to-wall distance.

The average number of beads n within the measurement volume and their residence time $\tau_D=w^2/D$ (where D is the self-diffusion coefficient of the bead) can be extracted from the autocorrelation function of the collected fluorescence intensity.

Runs belonging to different cells may slightly differ in absolute transit time and average number of beads due to small day-to-day variations in temperature, concentration or focus location. We accordingly normalized data from each cell by a reference point (τ_0, n_0) for (almost) unconfined beads, located at $e/2a=16.8$, for which excellent statistics were already achieved in the time frame of a single cell experiment.

For any location of the sphere–plane geometry where we measured n and τ_D, the wall-to-wall distance e was simultaneously measured using the interference pattern generated by the two confining surfaces (Newton's rings).

We note that e is known (and constant over the measurement spot size $2w\sim1\ \mu\mathrm{m}$) to better than 0.4%.

The first element we focused on is the evolution of the mean bead number with the confinement defined as $e/2a$. This evolution is shown in figure 3*b*, where we recover a linear behaviour for the averaged number of beads in the volume v as expected: $n=\langle c\rangle(\pi w^2)e$. This measurement provides an important check that the beam waist w and the average bead concentration $\langle c\rangle$ are constant over the different measurement locations. No depletion or adsorption due to bead–surface interaction is therefore detectable in our system, other than a layer of excluded volume close to the surfaces.[1] The thickness of this layer is measured from the extrapolation of the mean number of beads down to zero, obtained at $e/2a=1.2$, as shown in figure 3*b*. This layer is associated with the additional 'excluded volume' resulting from electrostatic repulsions between the wall and the beads.

We now move on to the measurement of the residence time—or reciprocally to the diffusion coefficient—of the beads as a function of the confinement $e/2a$, for different surface properties. As a starting point, we first considered the case of two hydrophilic confining walls, for which we expect the usual no-slip boundary condition to hold (Israelachvili 1986; Barrat & Bocquet 1999; Vinogradova & Yakubov 2003). In such a wetting situation, the bead mobility should be strongly reduced by the wall's proximity, as was already verified experimentally by a few groups (Faucheux & Libchaber 1994; Lin *et al.* 2000). Figure 4 summarizes our results for the measured diffusion times together with the theoretical predictions assuming no-slip boundary condition on both the walls (Saugey *et al.* 2005).

The agreement between experiments and theory with no-slip boundary condition on the walls is excellent up to the strongest confinements.

[1] Adsorption was found only when polystyrene beads were used together with hydrophobic surface: this couple was accordingly avoided in our measurements.

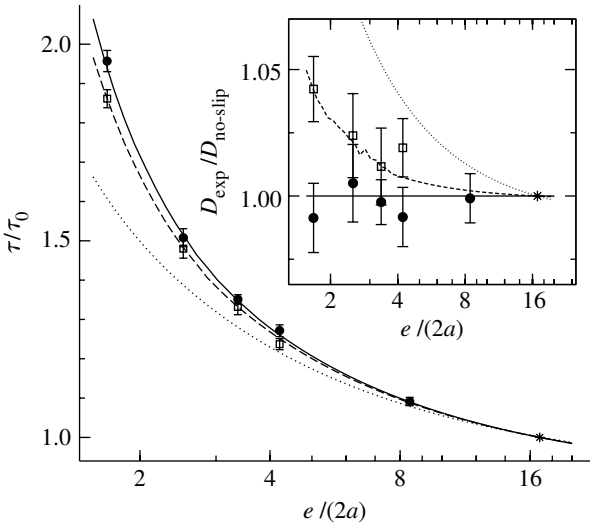

Figure 4. Evolution of the normalized diffusion time of silica beads ($2a$=218 nm) with confinement between a hydrophilic silica lens and a planar surface with varying surface property: filled circles, smooth hydrophilic surface (less than 1 nm peak-to-peak roughness); open squares, smooth hydrophobic wall (OTS-coated silica). Theoretical predictions are obtained using Comsol, assuming no-slip on the lens, and different boundary conditions on the plane: solid lines, no-slip; dashed lines, partial slip with b=18 nm. As a guide, the dotted line shows the theoretical prediction for b=100 nm slip length, illustrating the method sensitivity. Graph is taken from Joly *et al.* (2006).

We now move to non-wetting surfaces, for which very different partial slip behaviours have been reported. For that purpose, the silica plane was covalently coated using the same treatment as the one used for the dissipative measurements. In figure 4, the resulting residence time of the silica beads is plotted for different confinements against the previous results for wetting plane (plain silica). When beads are confined enough ($e/2a<5$), the residence times are measured to be systematically shorter close to the hydrophobic surfaces than to the hydrophilic ones. This effect is more easily captured when normalizing this evolution by the theoretical behaviour *in the absence of slip*: $D_{\text{exp}}(e/2a)/D_{\text{no-slip}}(e/2a)$. A failure of the no-slip boundary condition should result in a departure of this ratio from 1. This is indeed what is observed in the inset of figure 4 where the systematic trend described above is best evidenced. Moreover, it is possible to render this departure accurately by introducing a finite slip length b in the theoretical calculations (Saugey *et al.* 2005). The fitted behaviour agrees remarkably well with the experimental data providing a slip length on smooth OTS-coated silica planes of $b=18\pm5$ nm.

4. Micro- and nanovelocimetry

At first sight, the measurement of a slip length by velocimetry is elementary. It seems sufficient to measure the speed profiles close to the wall, to estimate the slip length. However, the expected order of magnitude of the slip length (less

than 1 μm) makes such a measurement rather challenging. The required accuracy in the speed profile resolution should be of the same order of magnitude as the slip length and is inaccessible by standard velocimetry. This has justified the development using particle microvelocimetry (μPIV) in microchannels, which provides direct measurements of the slip length, and more recently nano-PIV.

The first μPIV experiment in microchannels was reported by Tretheway & Meinhart (2002). In this work, water flows were driven through shallow microchannels with glass walls, either silanized or not. By observing the particle through the channel side walls, and focusing on the central region of the microchannel, these researchers could measure velocity profiles in two cases: wetting and non-wetting walls. In the former case, the slip lengths were indistinguishable from noise, while in the latter, slip lengths of the order of 1 μm or so were found. The error bar, estimated to 500 nm, was linked to the method of determination of the location of the channel walls. Our experiment was followed by a PIV study conducted with similar materials in shallow microchannels, but now looking at the flow from the larger side. The design allowed determination of the wall position within 30 nm accuracy. In this work, slip lengths below 100 nm were found, irrespective of whether the walls were wetting or non-wetting. The error bar was 100 nm. The discrepancy between the two experiments is not resolved yet.

Here, we describe the μPIV technique in some detail. PIV is based on the imaging of fluorescent particles within a flowing liquid: these particles are moved by the fluid and the determination of their motions allows a mapping of the flow. Ultrapure water was prepared with 200 nm fluorescent particles and the flow was driven in a 10×100 μm microchannel formed between polydimethylsiloxane and glass. Observation through a $100\times$ objective allows the observation of flowing particles in different planes by varying the plane in focus by a piezoelectric device (figure 5).

Speeds in the given planes were determined by the maximum of correlation between two successive frames. This method allows a reconstruction of a full speed profile within the microchannel with a resolution given by the objective depth of field z, which is typically 500 nm under experimental conditions used. The position of the wall was precisely determined by adjusting the signal collected from the tracers stuck on the wall, which allows pointing of the surface with 30 nm accuracy. A more detailed description of the methods and the results presented in the following discussion can be found in Joseph & Tabeling (2005).

Microvelocimetry was performed in flowing water either above the hydrophilic glass surfaces or the smooth silanized hydrophobic glass surfaces. The reconstruction of speed profiles (figure 6) leads to a measurement of the slip length given by the extrapolation of the speed profile to zero speed. This reveals that in both cases the slip length b is less than 100 nm: $b=50\pm50$ nm for the hydrophilic surfaces and $b=-35\pm100$ nm for the hydrophobic surfaces (Joseph & Tabeling 2005).

This measurement clearly sets an upper limit for the slip length value on the smooth hydrophobic surfaces and thus reduces drastically the possible range for the value of b compared with the previous experiments. Furthermore, recent theoretical predictions and experimental results have pointed to the possibility to create huge (more than 10 μm) slip lengths by the use of composite surfaces

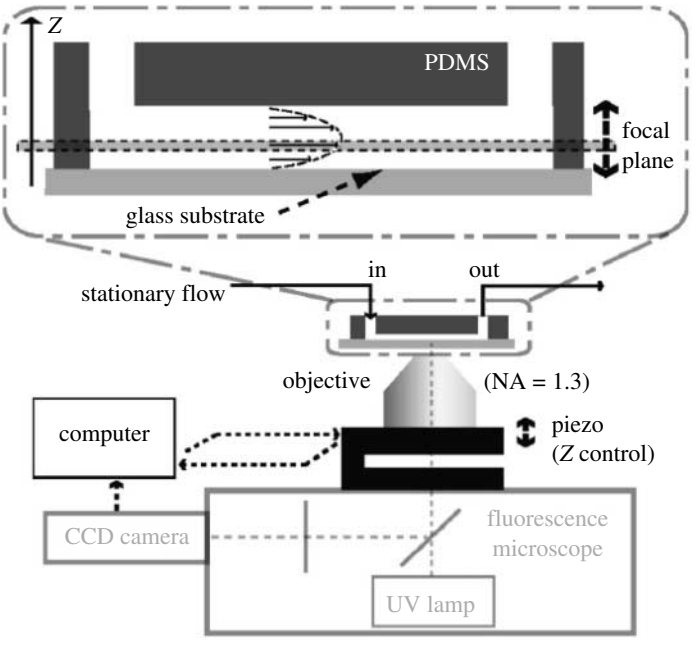

Figure 5. Schematic of the μPIV set-up (Joseph & Tabeling 2005). The focal plane is varied by moving the objective using the piezoelectric device. The large numerical aperture (NA) of the objective narrows the depth of field so as to image slices of approximately 500 nm thickness within the liquid.

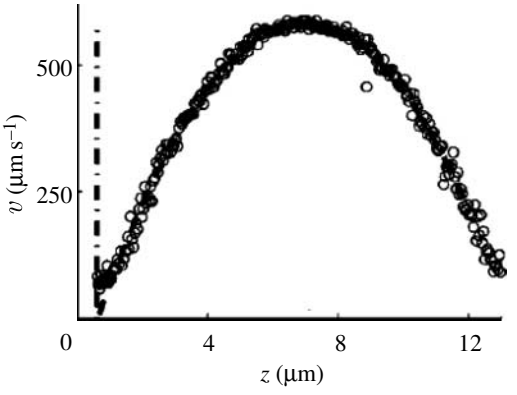

Figure 6. Example of speed profile (here on a hydrophobic surface) resolved by microvelocimetry. Deviations to Poiseuille's law close to the surface can be interpreted as an effect of hydrodynamic coupling of the particle to the solid surface.

(Choi & Kim 2006; Ybert *et al.* 2007). μPIV is a particularly appropriate method to measure the slippage on such surfaces, thanks to its ability to precisely reconstruct the speed profile with a submicrometre resolution, as has already been demonstrated on carbon nanotube-coated surfaces (Joseph *et al.* 2006).

As discussed above, μPIV provides an upper limit of the value of the slip length, but is unable to discriminate between the hydrophilic and smooth hydrophobic surfaces. This is due to a fundamental optical limitation of this

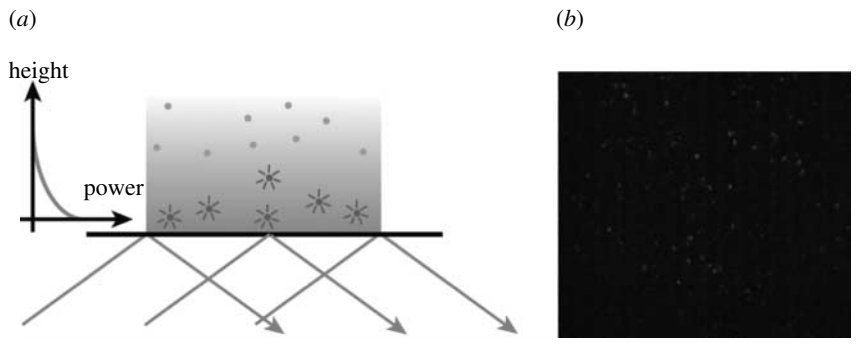

Figure 7. (*a*) Schematic of TIRF illumination. When the incidence angle is larger than the critical angle θ_c, light is totally reflected and only the tracers closer than a fraction of the wavelength are illuminated. (*b*) Typical image of the tracers within the microchannel under TIRF illumination.

method. The depth of the field δz of a standard immersion microscope is typically the wavelength and a better resolution than δz in the speed profiles measurement is thus not accessible.

New methods of PIV using total internal reflection fluorescence (TIRF) have thus been developed and are detailed here: when an interface between two media is illuminated by a light beam with an incident angle higher than the critical angle for total reflection, a non-propagating, or evanescent, field is created in the medium of lower refractive index (figure 7). The intensity of the illumination I in this medium is thus decreasing exponentially with the distance to the interface: $I = I_0 \exp(-z/L)$, where the penetration length L is given by $L = (\lambda/4\pi)\cdot(n_1^2 \sin^2 i_1 - n_2^2)$, where n_1 and n_2 are the respective refractive indexes of the first and second mediums; λ is the excitation wavelength; and i_1 is the incidence angle. Under standard experimental conditions, $L \sim 100$ nm, which results in restraining imaging of fluorescent tracers within an approximately 300 nm thick layer. The use of fluorescent probes within the fluid is thus particularly suitable for the investigation of the phenomena, such as slipping, occurring at the submicrometre distance of the surface.

This method of TIRF has been successfully used to observe the fluorescence recovery after photobleaching (FRAP) of the molecular probes in a flowing solution of alkanes. A fine modelling of the fluorescence recovery in a flow has allowed the first determination of the slip length for alkanes with 100 nm accuracy from the measurements of the recovery time as a function of the shear rate (Pit *et al.* 2000). However, this analysis relies on a modelling of diffusion–advection phenomena close to a surface and is a global measurement within an approximately 300 nm thick layer above the solid surface. It is thus not a direct measurement of the slip length and remains still controversial.

Recently developed methods of PIV using TIRF illumination have highlighted the possibility to locally probe a flow at a few hundreds of nanometres above a surface (Pouya *et al.* 2005; Huang *et al.* 2006). This has led to the proposal of the experimental approach detailed below to locally measure the properties of nanoflows in an approximately 300 nm layer with a resolution in the direction orthogonal to the flow of approximately 30 nm (Bouzigues & Tabeling 2007, submitted).

Ultrapure water was prepared with 20 nm diameter fluorescent particles. A flow of this liquid was driven in the microchannels as described above and movies were recorded (1000 images, acquisition rate of 25 Hz), while the tracers were illuminated through a high numerical aperture objective creating an evanescent wave (figure 7). Given the small size of the tracers compared with the illumination wavelength, the detection of tracers on each image of the movie was done by a method based on intercorrelation between the images and the point spread function of the optical system (Bonneau *et al.* 2005). This protocol allows a measurement of the position of single tracers in the horizontal plane with 30 nm accuracy and a measurement of the intensity, with an error negligible compared with the dispersion due to the tracer size variations. Given the structure of the evanescent illumination, the fluorescence intensity is a decreasing exponential function of the altitude, and its measurement provides a determination of the altitude of individual tracers. This allows tracking of single particles in three-dimensional tracking and the measurement of the speed of single tracers with a constant intensity between two successive frames, i.e. remaining at the same distance from the surface. Some tracers remain stuck to the surface and their intensity is the maximal emission intensity, which consequently allows an absolute determination of the altitude of the tracers.

The velocity of a single tracer is a balance between Brownian diffusion and the speed of drift due to the flow. By tracking thousands of tracers, the distribution of velocities at a given altitude was measured, which revealed the diffusion coefficient of the tracers and the speed of the flow at the same time. The reconstruction of the speed (figure 8*a*,*b*) and diffusion coefficient (figure 8*c*,*d*) profiles with a better resolution than 50 nm is thus possible by this method. These two quantities allow two independent determinations of the slip length b with an accuracy of 10 nm in both cases. The speed profile straightforwardly provides a direct measurement of b and the variations in the diffusion coefficient are a function of the slip length value due to hydrodynamic coupling of the particle with the surface (Goldman *et al.* 1967; Lauga & Squires 2005). It appears that on the hydrophilic surfaces no slippage was observed: $b = 3 \pm 7$ nm with the speed profile and $b = -1 \pm 12$ nm with the diffusion coefficient profile (figure 8*a*,*c*). On the contrary, the slip length is non-zero on the smooth hydrophobic surfaces produced by silanization of the glass surface. In that case, we measured a slip length $b = 29 \pm 11$ nm by the analysis of the speed profile and $b = 21 \pm 10$ nm by the analysis of the diffusion coefficient profile (figure 8*b*,*d*). These results are consistent with the slip length expected from the earlier results showing a reduction in water density at approximately 1 nm of the solid surface (Doshi *et al.* 2005).

The method outlined above is a direct way to measure the slip length. It is important to note that interpretations of the results are directly based on the speed profile analysis and consequently do not rely on any modelling of the behaviour of the fluid or the tracers in the vicinity of the surface. Moreover, this method is robust because it can be applied to a variety of systems even with poorly characterized surfaces. Different fluids can also be investigated; the only limitation is the possible aggregation of tracers in non-aqueous solvents. It is more generally possible to investigate nanoflows by total internal reflection velocimetry, by measuring the electrostatic effects within the Debye layer for example (Bouzigues & Tabeling 2007).

The question of slippage has also been addressed in other studies in different fluids, such as alkanes or benzene derivatives, either by colloidal AFM force measurement (Cho *et al.* 2004) or FRAP measurement (Pit *et al.* 2000). These

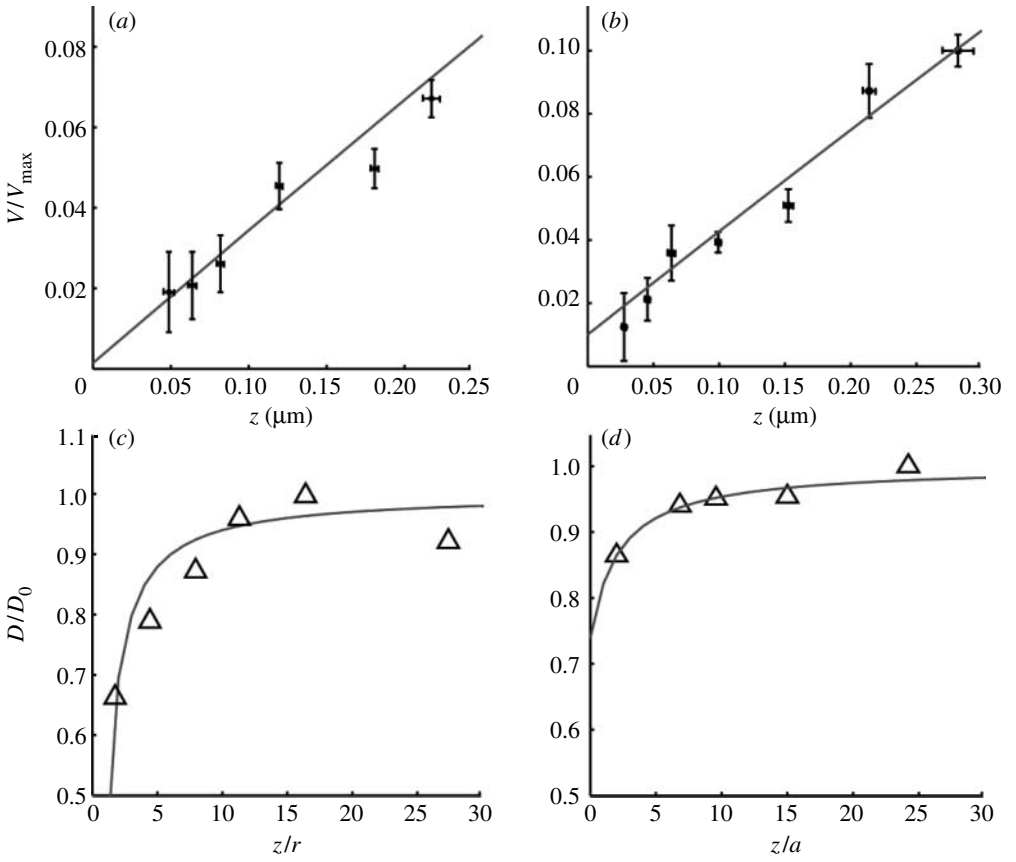

Figure 8. (a,b) Speed profiles on the hydrophilic and hydrophobic surfaces, respectively. Experimental points are represented by filled symbols, and the error bars indicate the dispersion of the speed due to diffusion, which is the only error source in the used conditions. The solid lines are nonlinear regressions by Poiseuille's law, $V_{\max}(1-(z-w)^2/(w+Ls)^2)$, where w is half of the channel width; $V_{\max}$ is the maximal speed measured by microvelocimetry; and b is the only free parameter. This fit yields $b=3$ and 29 nm. The eventual error on b is indicated in the text and corresponds to the 66% likelihood resulting from the fit. (c,d) Diffusion coefficient profiles on the hydrophilic and hydrophobic surfaces, respectively. Experimental points are shown by open triangles. Solid curves are fits by the theoretical variation law for the diffusion coefficient at the lowest order. The only free parameter is the slip length, which yields $b=-2$ and 21 nm.

results have pointed out the high dependence of the slip length on the nature of the liquid. For polar liquids such as water, wettability of the surface appears not to be the only relevant parameter for the slippage phenomenon, but that the dipole moment of the liquid is also essential. The standard interpretation of slippage as a result of a depletion layer due to the poor wettability of the surface is likely to be sufficient to account for non-polar liquid behaviour, but not for polar liquids such as water. For that reason, it is difficult to quantitatively compare the slippage properties of water with other fluids, such as alkanes. Further studies would be required to systematically investigate the slippage on different couples of liquids and solids, which lie beyond the scope of this paper.

5. Conclusion

In this paper, we reviewed the surface force apparatus and diffusion-based and PIV techniques (micro and nano) for measuring slip lengths. The three techniques consistently indicate slip lengths in the range of 15–30 nm for non-wetting surfaces and of the order of 1 nm or so for wetting surfaces. Pressure drop measurements (Choi *et al.* 2003) moreover provide slip length estimation of the same magnitude on the hydrophobic surfaces. There is no giant slippage effect, but still these estimates lie well above the numerical estimates.

Although there is progress in the instrumentation and in the consistency of the measurements (reported values of giant slip lengths have not received confirmation from improved instrumentation), we are still left with the experimental values lying one order of magnitude or so above those of the theory. Indeed, the computations were performed with Lennard-Jones potentials and simple surfaces, while most experiments were carried out with water as the working fluid and chemically modified walls. This must be kept in mind when comparing the experiments and computation. Nonetheless, at the moment, the quantitative discrepancy between theory and experiment must be considered as unresolved. Additional numerical work, taking the specificity of water into account, and perhaps details of the surface, might certainly shed light on the subject.

We acknowledge the support from ANR pNANO.

References

Barrat, J.-L. & Bocquet, L. 1999 Large slip effect at a nonwetting fluid–solid interface. *Phys. Rev. Lett.* **82**, 4671–4674. (doi:10.1103/PhysRevLett.82.4671)

Bonneau, S., Cohen, L. & Dahan. M. 2005 A multiple target approach for single quantum dot tracking. In *Proc. IEEE Int. Symp. Biological Imaging*, p. 664.

Bouzigues, C. & Tabeling. P. 2007 Particle image analysis: a new tool for the exploration of nanofluidic flows. *Proc. MicroTAS, Paris, France, 7–11 October 2007*, p. 0199.

Bouzigues C. & Tabeling, P. Submitted. Measuring velocity profiles and nanoparticle interactions at less than 100 nm from surfaces.

Cho, J. H., Law, B. M. & Rieutord, F. 2004 Dipole-dependent slip of Newtonian liquids at smooth solid hydrophobic surfaces. *Phys. Rev. Lett.* **92**, 166102. (doi:10.1103/PhysRevLett.92.166102)

Choi, C. H. & Kim, C. J. 2006 Large slip of aqueous liquid flow over a nanoengineered superhydrophobic surface. *Phys. Rev. Lett.* **96**, 066001. (doi:10.1103/PhysRevLett.96.066001)

Choi, C. H., Westin, K. J. A. & Breuer, K. S. 2003 Apparent slip flows in hydrophilic and hydrophobic microchannels. *Phys. Fluids* **15**, 2897. (doi:10.1063/1.1605425)

Cottin-Bizonne, C., Cross, B., Steinberger, A. & Charlaix, E. 2005 Boundary slip on smooth hydrophobic surfaces: intrinsic effects and possible artifacts. *Phys. Rev. Lett.* **94**, 056102. (doi:10.1103/PhysRevLett.94.056102)

Doshi, D. A., Watkins, E. B., Israelachvili, J. N. & Majewski, J. 2005 Reduced water density at hydrophobic surfaces: effect of dissolved gases. *Proc. Natl Acad. Sci. USA* **102**, 9458. (doi:10.1073/pnas.0504034102)

Einstein, A. 1905 Über die von der molekularkinetischen Theorie der Wärme geforderte Bewegung von in ruhenden Flüssigkeiten suspendierten Teilchen. *Ann. Phys.* **17**, 549. (doi:10.1002/andp.19053220806)

Faucheux, L. P. & Libchaber, A. J. 1994 Confined Brownian motion. *Phys. Rev. E* **49**, 5158. (doi:10.1103/PhysRevE.49.5158)

Goldman, A. J., Cox, R. G. & Brenner, H. 1967 Slow viscous motion of a sphere parallel to a plane wall. I. Motion through a quiescent fluid. *Chem. Eng. Sci.* **22**, 637. (doi:10.1016/0009-2509(67)80047-2)

Huang, P., Guasto, J. S. & Breuer, K. S. 2006 Direct measurement of slip velocities using three-dimensional total internal reflection velocimetry. *J. Fluid. Mech.* **566**, 447. (doi:10.1017/S0022112006002229)

Israelachvili, J. N. 1986 Measurement of the viscosity of liquids in very thin films. *J. Colloid Interface Sci.* **110**, 263. (doi:10.1016/0021-9797(86)90376-0)

Joly, L., Ybert, C. & Bocquet, L. 2006 Probing the nanohydrodynamics at liquid–solid interfaces using thermal motion. *Phys. Rev. Lett.* **96**, 046101. (doi:10.1103/PhysRevLett.96.046101)

Joseph, P. & Tabeling, P. 2005 Direct measurement of the apparent slip length. *Phys. Rev. E* **71**, 035303. (doi:10.1103/PhysRevE.71.035303)

Joseph, P., Cottin-Bizonne, C., Benoît, J.-M., Ybert, C., Journet, C., Tabeling, P. & Bocquet, L. 2006 Slippage of water past superhydrophobic carbon nanotube forests in microchannels. *Phys. Rev. Lett.* **97**, 156104. (doi:10.1103/PhysRevLett.97.156104)

Lauga, E. & Squires, T. 2005 Brownian motion near a partial-slip boundary: a local probe of the no-slip condition. *Phys. Fluids* **17**, 103102. (doi:10.1063/1.2083748)

Lin, B., Yu, J. & Rice, S. A. 2000 Direct measurements of constrained Brownian motion of an isolated sphere between two walls. *Phys. Rev. E* **62**, 3909. (doi:10.1103/PhysRevE.62.3909)

Mason, T. G. & Weitz, D. A. 1995 Optical measurements of frequency-dependent linear viscoelastic moduli of complex fluids. *Phys. Rev. Lett.* **74**, 1250. (doi:10.1103/PhysRevLett.74.1250)

Navier, C. L. M. H. 1822 Memoire sur les lois du mouvement des fluides. *Mem. Acad. Sci.* **6**, 389–440.

Pit, R., Hervet, H. & Leger, L. 2000 Direct experimental evidence of slip in hexadecane: solid interfaces. *Phys. Rev. Lett.* **85**, 980. (doi:10.1103/PhysRevLett.85.980)

Pouya, S., Koochesfahani, M., Snee, P., Bawendi, M. & Nocera, D. 2005 Single quantum dot (QD) imaging of fluid flow near surfaces. *Exp. Fluids* **39**, 784. (doi:10.1007/s00348-005-0004-x)

Restagno, F., Crassous, J., Charlaix, E., Cottin-Bizonne, C. & Monchanin, M. 2002 A new surface forces apparatus for nanorheology. *Rev. Sci. Instrum.* **73**, 2292. (doi:10.1063/1.1476719)

Saugey, A., Joly, L., Ybert, C., Barrat, J.-L. & Bocquet, L. 2005 Diffusion in pores and its dependence on boundary conditions. *J. Phys. Condens. Matter* **17**, S4075. (doi:10.1088/0953-8984/17/49/005)

Tabeling, P. 2003 *Une introduction à la microfluidique Collections Echelles.* Paris, France: Editions Belin.

Thompson, P. A. & Troian, S. M. 1997 A general boundary condition for liquid flow at solid surfaces. *Nature* **389**, 360. (doi:10.1038/39475)

Tretheway, D. & Meinhart, C. 2002 Apparent fluid slip near hydrophobic microchannel walls. *Phys. Fluids* **14**, 9. (doi:10.1063/1.1432696)

Vinogradova, O. I. 1995 Drainage of a thin liquid-film confined between hydrophobic surfaces. *Langmuir* **11**, 2213. (doi:10.1021/la00006a059)

Vinogradova, O. I. & Yakubov, G. E. 2003 Dynamic effects on force measurements. 2. Lubrication and the atomic force microscope. *Langmuir* **19**, 1227. (doi:10.1021/la026419f)

Ybert, C., Barentin, C., Cottin-Bizonne, C., Joseph, P. & Bocquet, L. 2007 Achieving large slip with superhydrophobic surfaces: scaling laws for generic geometries. *Phys. Fluids* **19**, 123601. (doi:10.1063/1.2815730)